JTTEE5 10:293-300

Thermal Stability of Nanostructured Cr_3C_2-NiCr Coatings

Jianhong He, Michael Ice, Julie M. Schoenung, Dong H. Shin, and Enrique J. Lavernia

(Submitted 28 February 2000; in revised form 15 June 2000)

The thermal stability behavior of nanostructured Cr_3C_2-NiCr coatings was investigated. The nanostructured Cr_3C_2-NiCr coatings, synthesized using mechanical milling and high-velocity oxygen fuel (HVOF) thermal spraying, were thermally exposed in air at 473, 673, 873, and 1073 K for 8 h. The results show that microhardness of the conventional coating increased slightly with increasing temperature, while that of the nanostructured coating drastically increased from 1020 to 1240 HV_{300} for the same temperature increases. Heat treatment led to increases in scratch resistance and decreases in the coefficient of friction for the nanostructured Cr_3C_2-NiCr coatings. A high density of Cr_2O_3 oxide particles with average size of 8.3 nm was found in the nanostructured coatings exposed to high temperatures, which is thought to be responsible for the observed increase in microhardness and scratch resistance and the decrease in the coefficient of friction of the nanostructured coatings.

Keywords HVOF thermal spraying, nanostructured materials, precipitation, thermal stability

1. Introduction

The intrinsically high physical and mechanical properties of nanostructured materials have led to a significant interest in the research and development of various nanostructured materials applications. Through a combination of high-velocity oxygen fuel (HVOF) spraying technology and ball milling, a process that allows for production of nanostructured feedstock powders, several nanostructured coatings have been successfully sprayed.[1–4] Coatings based on a Cr_3C_2-NiCr composition are commonly used for wear and corrosion resistant applications at elevated temperatures;[5–11] therefore, the thermal stability response of these coatings is a critical factor in determining the coating's performance. Thus, the primary objective of the present paper is to report on the thermal stability behavior of nanostructured Cr_3C_2-NiCr coatings.

2. Experimental Procedure

Prealloyed Cr_3C_2-NiCr powders (Dialloy 3004 blended Cr_3C_2-25 (Ni20Cr), produced by Sulzer Metco Inc. (Westbury, NY, US) were chosen for this study. The powders were immersed in Hexane (Union Process, Akron, OH) [$H_3C(CH_2)_4CH_3$] and mechanically milled with a modified Szegvari attritor model B at a rate of 180 rpm for 20 h in a stainless steel tank with stainless steel balls. X-ray diffraction and transmission electron microscope (TEM) observations indicated that the as-milled powder is a nanocomposite of the NiCr phase and Cr_3C_2 particles. The average grain size of the nanostructured powder was 15 nm.[12] The chemical compositions of the nano-structured and the conventional (as-received) Cr_3C_2-NiCr powders are shown in Table 1.

These two powders were used as feedstock powder to synthesize nanostructured and conventional Cr_3C_2-NiCr coatings, respectively, by HVOF thermal spraying. To prepare Cr_3C_2-NiCr coatings, a Sulzer Metco Diamond Jet HVOF thermal spray facility was used. The main constituents of this facility are described in detail elsewhere.[3,4] The spraying parameters are summarized in Table 2.

The as-sprayed coatings were thermally exposed in air at 473, 673, 873, and 1073 K for 8 h. The average microhardness was taken on the cross section using a Buehler Micromet 2004 Microhardness tester (Buehler, Lake Bluff, IL) with a load of 300 g. The friction coefficient and scratch resistance of the nanostructured coatings were measured at Center for Tribology, Inc. (Mountain View, CA) using a CETR Micro-Tribometer. The scratch head was a sapphire ball with a radius of 0.75 mm, and the scratch tests were performed under a scratch rate of 535 mm/min and scratch normal load of 5 N. The examinations for cross-sectional microstructure of the coatings and x-ray mapping were conducted using a Philips XL 30 field emission gun (FEG) scanning electron microscope (SEM) (Philips Electronic Instruments Corp., Mahwah, NJ). After removal of the substrate by polishing, TEM specimens were prepared by cutting out a section of the coating and forming 3 mm diameter disks. The disks were dimpled to approximately 30 μm in thickness using a dimpler fitted with diamond grinders. The grinding size descended progressively from a 6 μm grade, to 3 μm, and finally to a 1 μm grade. The final thinning perforation process was performed using an argon ion mill. With the prepared samples, TEM observations were carried out on a Philips CM20 microscope operated at 200 keV.

3. Results and Discussion

3.1 Influence of Thermal Exposure on Mechanical Properties of Coatings

The cross-sectional microstructures of the as-sprayed conventional and nanostructured Cr_3C_2-NiCr coatings are shown in

Jianhong He, Michael Ice, Julie M. Schoenung, and **Enrique J. Lavernia,** Department of Chemical and Biochemical Engineering and Materials Science, School of Engineering, University of California, Irvine, Irvine, CA 92697-2575. **Dong H. Shin,** Department of Metallurgy and Materials Science, Hanyang University, Ansan, South Korea. Contact e-mail: lavernia@uci.edu.

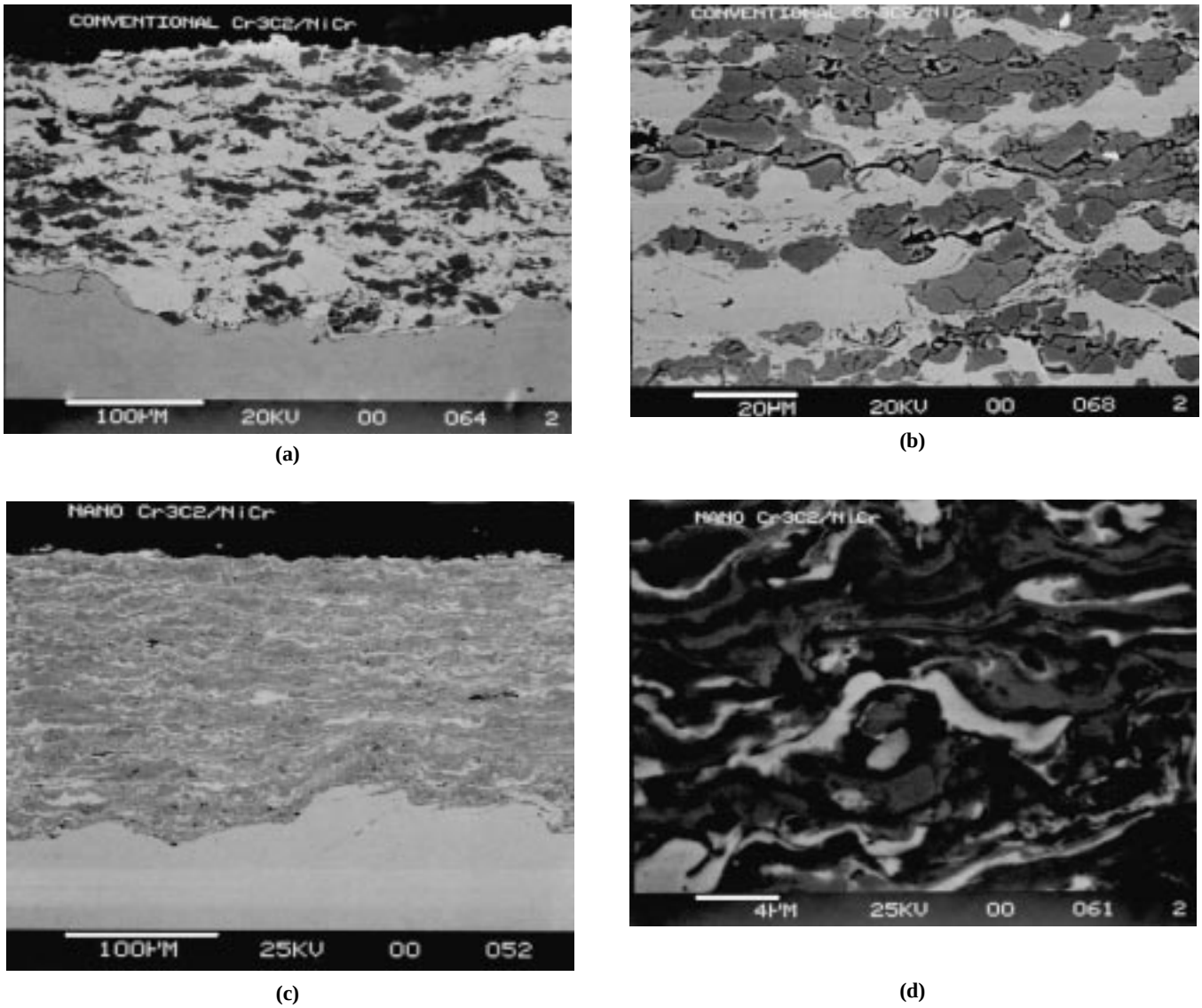

Fig. 1 Microstructure of Cr_3C_2-25(Ni20Cr) coatings. (**a**) Conventional coating, (**b**) magnification of (a), (**c**) nanostructured coating, and (**d**) magnification of (c)

Table 1 Chemical composition of Cr_3C_2-NiCr powders (wt.%)

Powder	Cr	Ni	C	N	O
Conventional	70.0	19.2	9.83	0.20	0.21
Nanostructured	64.3	18.8	9.36	0.51	1.93

Table 2 Spraying parameters used to produce Cr_3C_2-NiCr coatings

Gas	Pressure (MPa)	FMR(a)	GSFR(b)	Parameter	Setting
Air	0.69	48	6740	Powder feed rate	0.315 g/s
Propylene	0.69	40	1384	*X-Y* traverse speed	1.016 m/s
Nitrogen	1.034	55	220	Spraying distance	0.203 m
Oxygen	1.034	40	4546	. . .	. . .

(a) FMR: flow meter reading
(b) GSFR: gas standard flow rate (cm^3/s)

Fig. 1. The thickness of the coatings is approximately 200 μm. A uniform and dense microstructure is observed in the nanostructured coatings, compared to the conventional Cr_3C_2-NiCr coating that is observed to have an inhomogeneous microstructure. The TEM bright-field image of the as-sprayed nanostructured coating and the corresponding dark-field image are shown in Fig. 2. The average carbide particle size is approximately 24 nm. This indicates that the coating is inherently nanostructured.

The measured microhardness values, each microhardness value being obtained from an average value of 30 tests, for both conventional and nanostructured Cr_3C_2-NiCr coatings are plotted in Fig. 3. The microhardness of the as-sprayed coatings in-

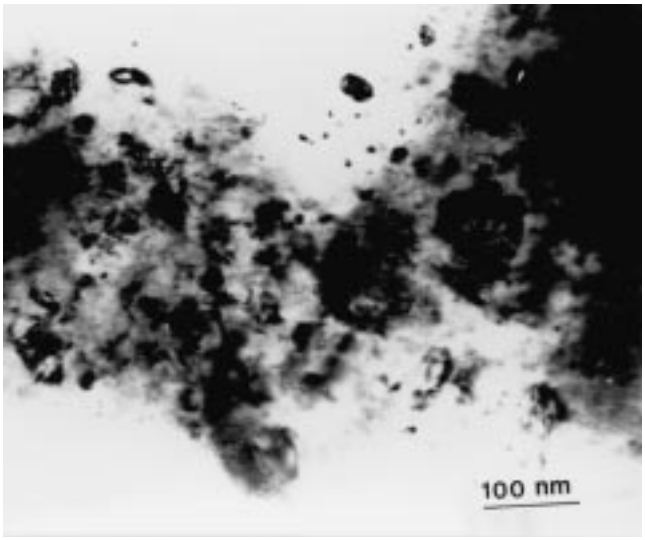

(a)

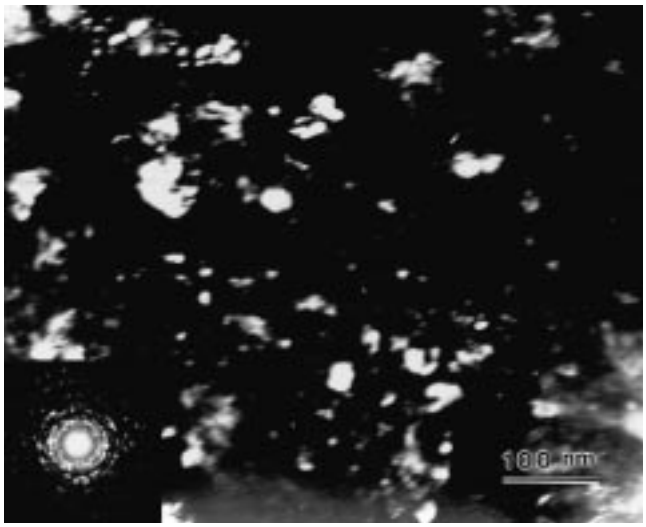

(b)

Fig. 2 TEM observation of nanostructured Cr_3C_2-25(Ni20Cr) coatings: (**a**) bright-field image and (**b**) dark-field image

creases from a value of 846 for the conventional coating to 1020 HV_{300} for the nanostructured coating. Hence, the nanostructured coating exhibits a 20.5% increase in microhardness as compared with the corresponding conventional coating. It has been reported that the hardness of nanostructured materials often exhibits a two- to fivefold increase compared to that of the corresponding conventional materials, although it is lower than that predicated using the classical Hall-Petch equation.[13–15] Farhat *et al.*[16] have also shown that Al with grain size in the range of 15 to 100 nm follows the Hall-Petch relationship and its hardness increases with decreasing grain size. Therefore, the observed increase in hardness of the as-sprayed nanostructured Cr_2C_3-NiCr coating is attributed to intrinsic high mechanical properties of nanostructured materials. However, the observed increase of hardness in the nanostructured coatings is evidently less than the comparable increase reported for bulk materials.

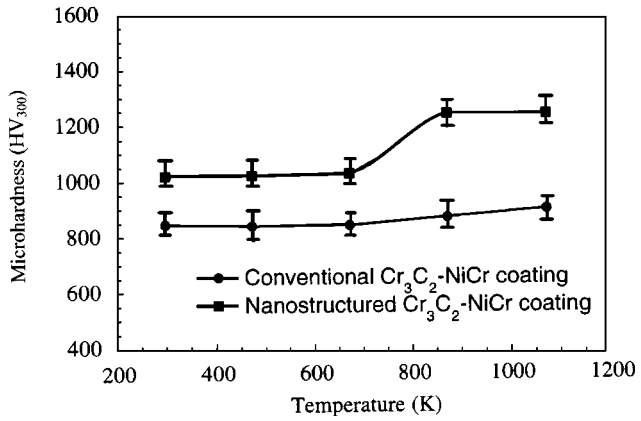

Fig. 3 Variation of microhardness of Cr_3C_2-25(Ni20Cr) coatings with heat treatment temperature

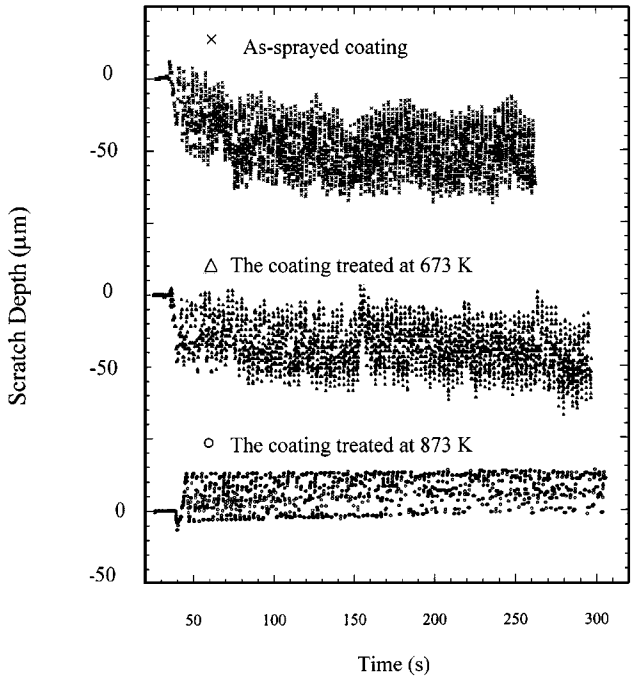

Fig. 4 Influence of heat treatment temperature on scratch resistance of nanostructured coatings

This is thought to be associated with the microstructural characteristics of the coatings. The presence of a high volume fraction of porosity, oriented microstructural constituents, and intersplat regions is believed to significantly influence the mechanical properties of the coatings. In related studies involving nanostructured Ni, Inconel 718, and AISI 316 stainless steel coatings, microhardness values increased by 20, 60, and 36%, respectively, as compared to the corresponding conventional coatings.[2]

The microhardness of the conventional coating exhibits a limited increase with exposure at entire temperature ranges, while that of the nanostructured coating drastically increases from 1020 to 1240 HV_{300} in the temperature range 700 to 900 K, and then approaches a constant value.

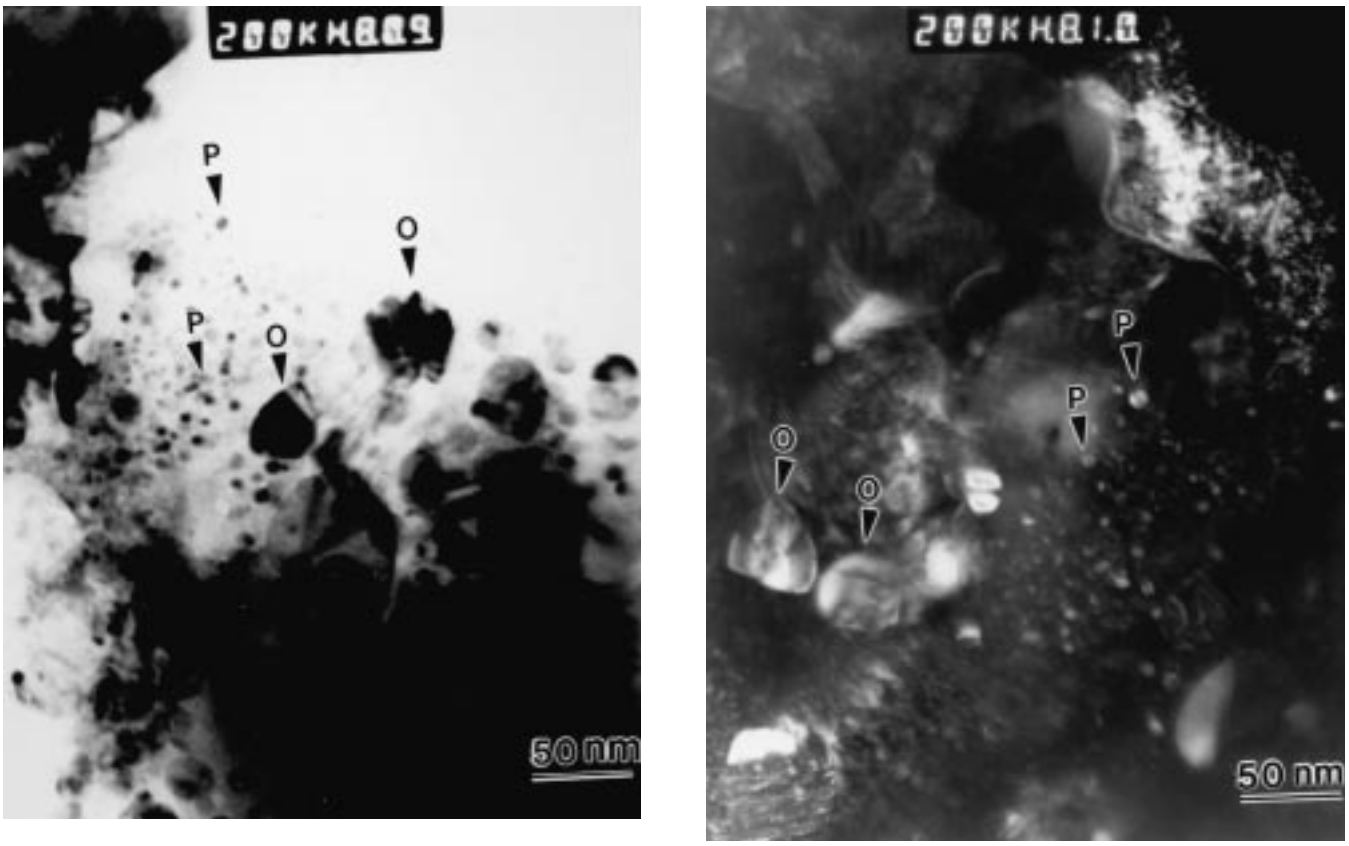

(a) **(b)**

Fig. 5 Precipitates in the nanostructured Cr_3C_2-25(Ni20Cr) coating. Arrows O and P indicate original carbide particles and precipitates, respectively. (**a**) Bright-field image and (**b**) dark-field image

The relationship between scratch depth and time under a normal load of 5 N is shown in Fig. 4. A reading of scratch depth (vertical ordinate of the scratch head) was taken every 0.01 s during the tests, which were automatically controlled by a computer; thus, a few tens of thousands of data illustrating the relation between scratch depth and time were recorded during a single scratch run. The scratch depth values distribute in a rather wide range because of microvibration of the system during tests. The average scratch depth decreases with increasing heat treatment temperature. The as-sprayed nanostructured coating produces an average scratch depth of approximately 50 μm, whereas a depth of around 27 μm is found in the nanostructured coating treated at 673 K. No scratch marks were found in the nanostructured coating treated at 873 K under the present experimental conditions. The results of scratch depths are supported by the measured microhardness values. Coefficients of friction, under the mode of the "ball on disk" friction, were also obtained from the scratch tests and are 0.216, 0.205, and 0.183 for as-sprayed coating, coating exposed at 673 K, and coating treated at 873 K, respectively. Compared with the coefficient of friction in the as-sprayed nanostructured coating, reduced coefficients of friction are observed as heat treatment temperature increases.

A number of publications report the application of Cr_3C_2-NiCr coatings at elevated temperatures.[5–11] In a related study,[8] the Cr_3C_2-NiCr was heated at 1123 K for 2 h and the results showed that the hardness on cross sections did not decrease even though Cr_2O_3 was detected by x-ray diffraction. The results published by Fukuda and Kumon[10] showed that heat treatment at 923 K for 1000 h yielded a maximum hardness value of 1100 for D-gun sprayed Cr_3C_2-NiCr coatings. In their experiments, hardness was measured at 900 Hv for the as-sprayed coatings, 1100 for the coatings heated at 923 K for 1000 h, and 1000 for the coatings heated at 1123 K for 1000 h. Cr_3C_2-NiCr coatings with the highest hardness offered the best abrasive and erosive wear resistance.[7] Therefore, it can be concluded that, on the basis of published studies and the present experimental results, a suitable postspraying heat treatment is beneficial for properties of both conventional and nanostructured Cr_3C_2-NiCr coatings.

3.2 Phase Transformation in Coatings during Thermal Exposure

Phase transformations in conventional Cr_3C_2/NiCr coatings at high temperatures have been reported.[8–12] Lai[11,17] showed that there are structural changes in carbides from Cr_3C_2 to Cr_7C_3 to $Cr_{23}C_6$ during exposure to elevated temperatures. Relative thermodynamic stability of carbides was determined by their standard free energies of formation. Cr_3O_2 was commonly detected by x-ray diffraction in the Cr_3C_2-NiCr coatings exposed to air,[8,10] high-pressure helium,[11,17] and N_2-3% H_2 gas[9] at high temperatures.

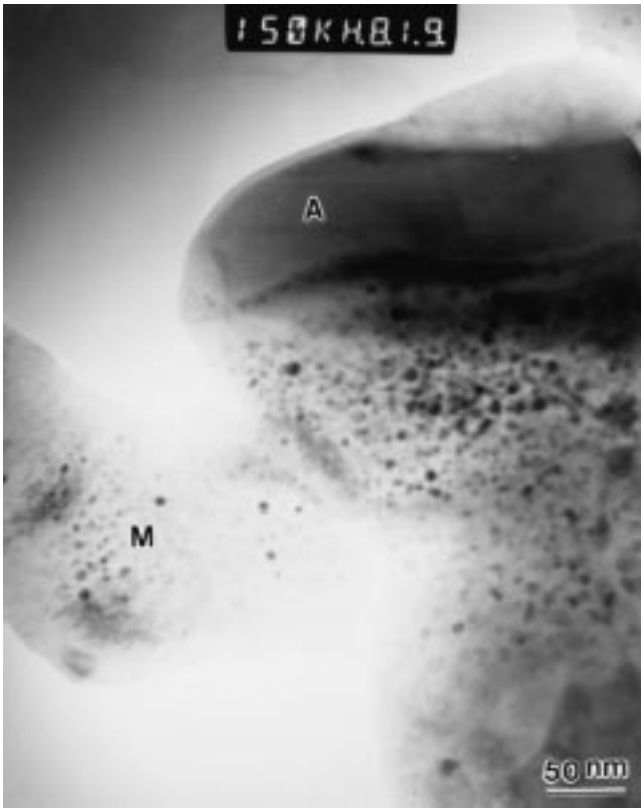

(a)

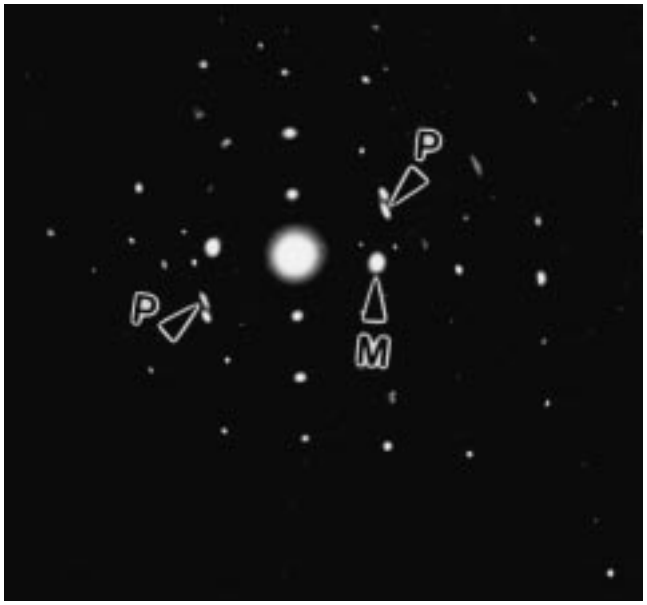

(b)

(c)

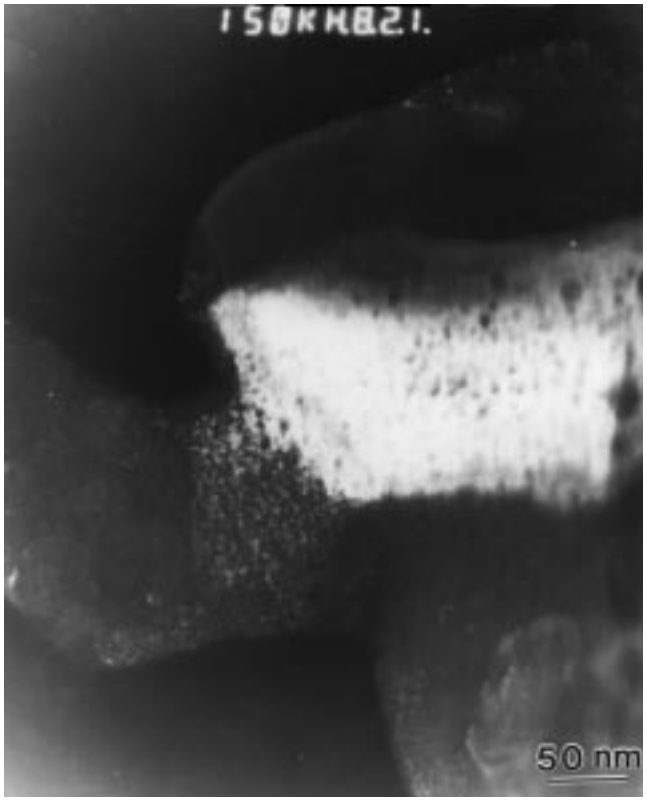

(d)

Fig. 6 TEM examination of precipitates and matrix in the nanostructured coating exposed at 1073 K. (**a**) Bright-field image; (**b**) SAD pattern of area M in (a), **B** = [$\bar{1}$12]; (**c**) Dark-field image of the precipitates using the P spot in (b); (**d**) Darkfield image of the matrix, using the M spot in (b), illustrating grains

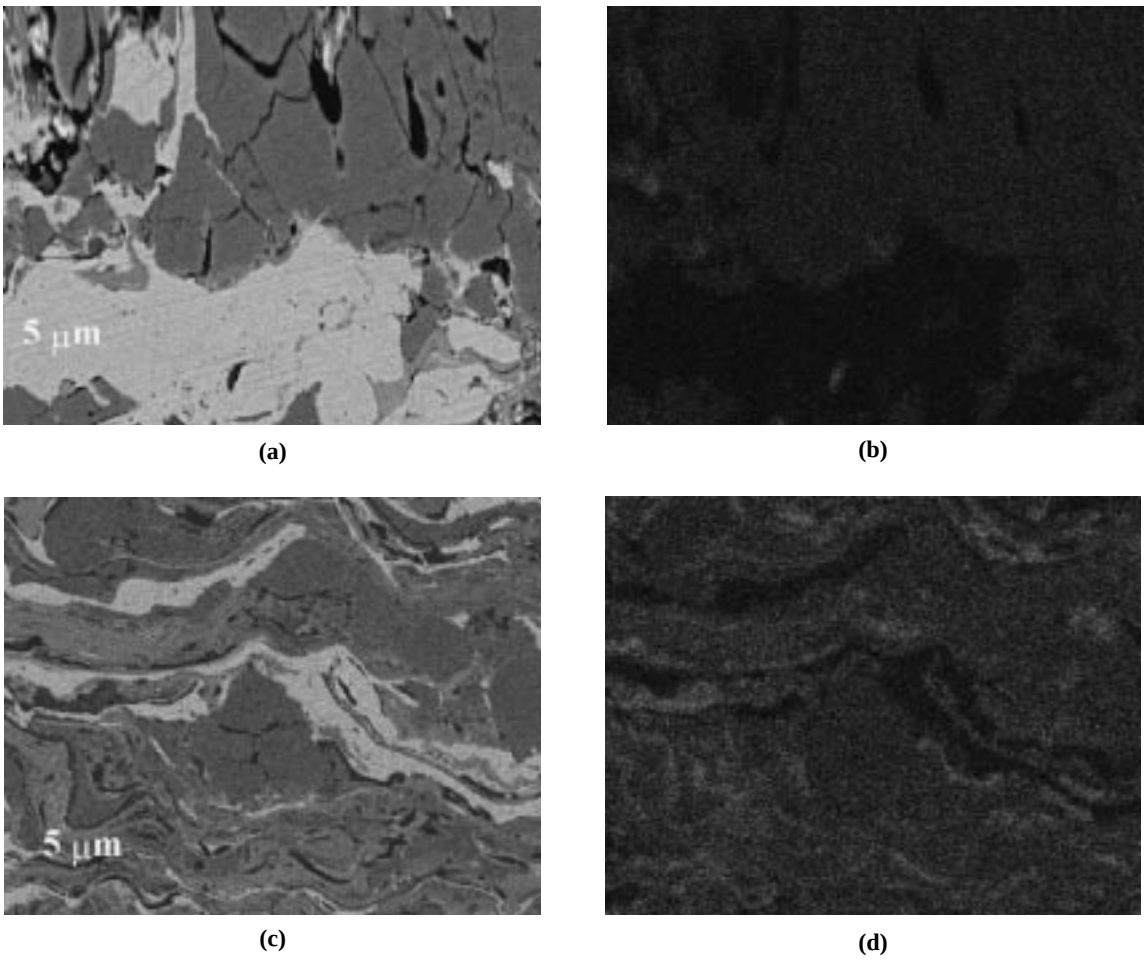

Fig. 7 X-ray oxygen element mapping of the as-sprayed coatings. (**a**) SEM backscattered electron image of conventional coating, (**b**) corresponding oxygen element map, (**c**) SEM backscattered electron image of nanostructured coating, and (**d**) corresponding oxygen element map

Figure 5(a) and (b) show the TEM bright-field image, dark-field image of the nanostructured coating treated at 1073 K, in which arrows O and P indicate original carbide particles and precipitates, respectively. The spherically shaped precipitates nucleate and grow in the matrix rather than on the original carbide particles. The average size of the original carbide particles increases from 24 nm in the as-sprayed coating to 39 nm in the thermally treated coating, and precipitates have an average size of 8.3 nm. The relationship between the matrix and precipitates is shown in Fig. 6. Figure 6(a) shows a TEM bright-field image. Arrow M indicates the matrix containing a high density of precipitates, and arrow A indicates an original amorphous phase.[4] Figure 6(b) is a selected area diffraction (SAD) pattern of the matrix M consisting of two sets of diffraction spots from the fcc matrix and hexagonal (a = 0.4954 nm, and c = 13.584 nm) Cr_2O_3 particles. The electron beam illuminates in the [$\bar{1}$12] orientation of the matrix. The P arrows indicate the diffraction spots {220} of Cr_2O_3, and arrow M indicates diffraction spots {220} of the fcc matrix; thus, the present results explicitly show that nanosized precipitates are Cr_2O_3 particles. The dark-field image of the precipitates was taken using a P spot and is shown in Fig. 6(c); the spherically shaped precipitates are densely distributed in the matrix. The dark-field image of the matrix taken using the M spot is shown in Fig. 6(d). The average grain size of the matrix is approximately 150 nm.

X-ray mapping was conducted using the Philips XL 30 FEG SEM; the results, shown in Fig. 7 and 8, show that in the as-sprayed coatings, high oxygen content is observed in the nanostructured coating, while there is a lower oxygen content in the conventional coating. In the coatings exposed at 873 K, high oxygen contents are found in both conventional and nanostructured coatings. Thus, oxidation occurs in the carbide phases of Cr_3C_2-NiCr coatings exposed to air at high temperatures regardless of original oxygen content in the coatings. Oxygen is absent in the NiCr binder phase. The observed difference in the oxygen content in the as-sprayed nanostructured and the as-sprayed conventional coatings is attributed to the presence of different oxygen contents in the starting powders, as well as oxygen entrainment during spraying. There is a high oxygen content (1.93 wt.%, Table 1) in the nanostructured powder. In a related study, Lau *et al.*[1] indicated that the surface area per unit weight of the milled Ni powder increased by approximately 7 times compared with that of the corresponding conventional powder. Thus, a larger surface area per unit weight of nanostructured powder also increases the absorption of oxygen during spraying. In addition, oxygen entrainment increases with increasing pow-

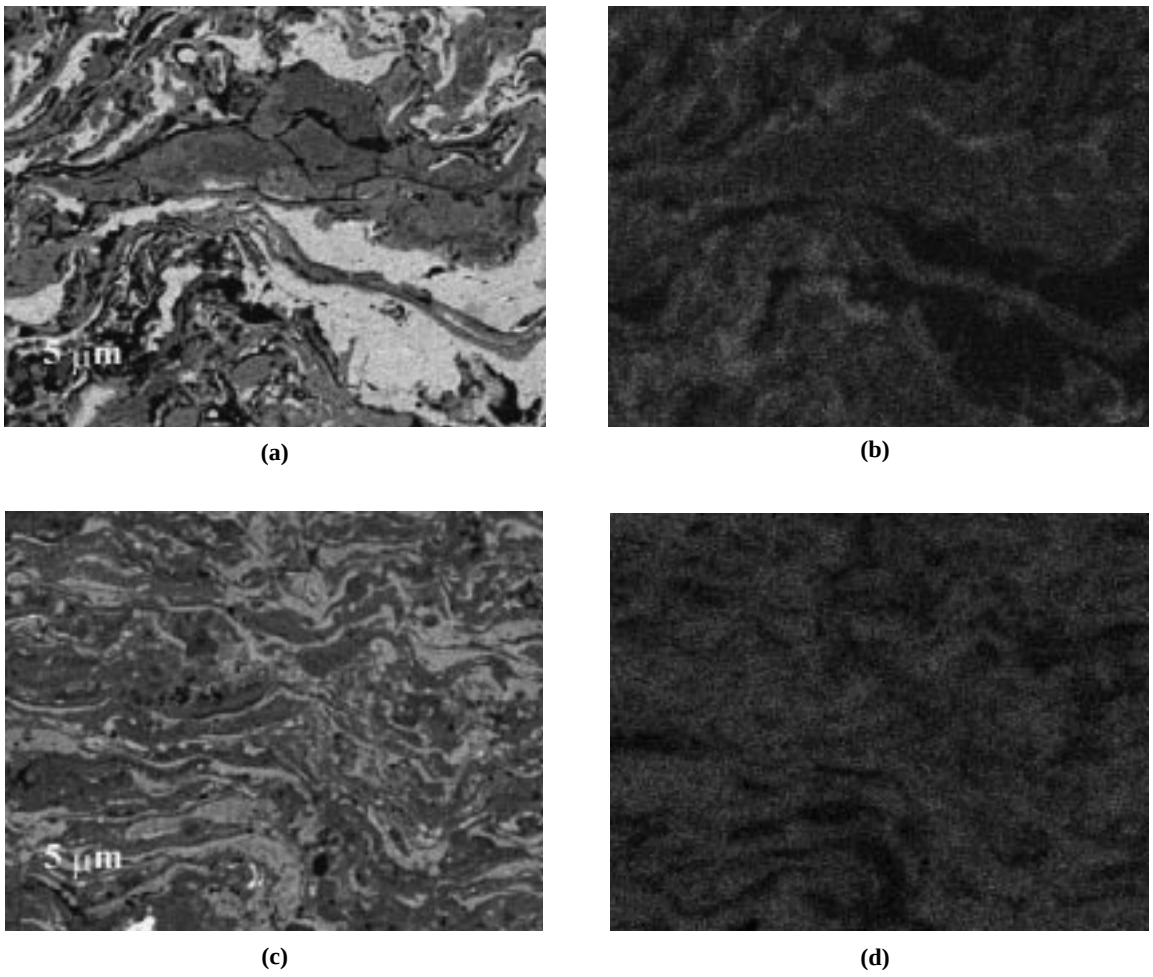

Fig. 8 X-ray oxygen element mapping result of the coatings exposed at 873 K: (**a**) SEM backscattered electron image of the conventional coating, (**b**) corresponding oxygen element map, (**c**) SEM backscattered electron image of the nanostructured coating, and (**d**) corresponding oxygen element map

der temperature during spraying. Related study results[3] showed that WC-12% Co nanostructured powder experienced approximately 400 K higher temperature than the corresponding conventional powder during HVOF spraying. Therefore, oxygen is pronouncedly entrained in the nanostructured coatings during spraying.

On the basis of the distribution of oxygen in the coatings, it is proposed that the observed Cr_2O_3 particles in the nanostructured coatings evolve as follows. First, there is high oxygen potential in the as-sprayed nanostructured coatings, due to the presence of oxygen in the starting powder, as well as oxygen entrainment during thermal spraying. Second, oxygen reacts with chromium to form CrO, CrO_2, CrO_3, Cr_2O_3, and Cr_3O_4; however, CrO, CrO_2, CrO_3, and Cr_3O_4 are metastable and/or present only under a high pressure.[18] Therefore, during thermal exposure, Cr_2O_3 is directly formed from the following chemical reaction:

$$4Cr_3C_2 + 17O_2 = 6Cr_2O_3 + 8CO_2 \quad \text{(Eq 1)}$$

The formation of the Cr_2O_3 phase is confirmed by the TEM analysis that reveals the presence of a diffraction pattern from the hexagonal ($a = 0.4954$ nm, and $c = 13.584$ nm) Cr_2O_3 phase. The Cr_2O_3 phase, with the Gibbs free energy of formation of per mole volume of $\Delta G = -251.70$ kilocalories,[19] is relatively stable. Third, the nucleation and growth of the Cr_2O_3 phase uniformly occurs throughout the coating, because most of the oxygen is primarily observed in the nano-Cr_3C_2 particles (Fig. 7 and 8) that are uniformly distributed in the coating. Therefore, this internal oxidation process leads to the formation of fine (8.3 nm) and dispersed Cr_2O_3 precipitates in the nanostructured Cr_3C_2 coatings.

The increase in microhardness of Cr_3C_2-NiCr coatings exposed to high temperatures is attributed to the precipitation of oxide phases, as described above. Particularly, in the nanostructured coatings, the high density of nanosized oxide particles within the matrix led to significant increases in the microhardness and, hence, an increase in scratch resistance.

4. Conclusions

In conclusion, the experimental results show that microhardness of the conventional coating increased slightly with increasing temperature, while that of the nanostructured coating

drastically increased from 1020 to 1240 HV_{300} for the same temperature increases. Heat treatment led to increases in scratch resistance and decreases in the coefficient of friction for the nanostructured Cr_3C_2-NiCr coatings. A high density of Cr_2O_3 oxide particles with average size of 8.3 nm were found in the nanostructured coatings exposed to high temperatures, which explained the increase in microhardness and scratch resistance and the decrease in the coefficient of friction of the nanostructured coatings.

Acknowledgments

The authors gratefully acknowledge financial support provided by the Office of Naval Research (ONR Grant Nos. N00014-94-1-0017, N00014-98-1-0569, and N0001497-1-0844). In addition, the authors thank The Center for Tribology, Inc. for measuring the friction coefficient and scratch resistance of the coatings.

References

1. M.L. Lau, H.G. Jiang, W. Nuchter, and E. J. Lavernia: *Phys. Status Solidi (a),* 1998, vol. 166, pp. 257-68.
2. E.J. Lavernia, M.L. Lau, and H.G. Jiang: in *Thermal Spray Processing Nanocrystalline Materials, Nanostructured Materials,* G. M. Chow and N.I. Noskova, eds., Kluwer Academic Publishers, Dordrecht, The Netherlands, 1998, pp. 283-302.
3. J. He, M. Ice, and E.J. Lavernia: *Metall. Mater. Trans. A,* 2000, vol. 31A, p. 553.
4. J. He, M. Ice, and E.J. Lavernia: *Metall. Mater. Trans. A,* 2000, vol. 31A, pp. 555-64.
5. J.M. Guilemany and J.A. Calero: in *Thermal Spray: A United Forum for Scientific and Technological Advances,* C.C. Berndt, ed., ASM International, Materials Park, OH, 1997, pp. 717-21.
6. P. Vuoristo, K. Niemi, T. Mantyla, L.M. Berger, and M. Nebelung: in *Thermal Spray Science & Technology,* C. C. Berndt and S. Sampath, eds., ASM International, Materials Park, OH, 1995, pp. 309-15.
7. L. Russo and M. Dorfmann: in *Thermal Spraying: Current Status and Future Trends,* A. Ohmori, ed., High Temperature Society of Japan, Osaka, Japan, 1995, pp. 681-86.
8. M. Sasaki: in *Thermal Spray: International Advances in Coatings Technology,* C.C. Berndt, ed., ASM International, Materials Park, OH, 1992, pp. 165-70.
9. S.Y. Hwang and B.G. Seong: in *Thermal Spray Coatings: Research, Design and Applications,* C.C. Berndt and T. F. Bernecki, eds., ASM International, Materials Park, OH, 1993, pp. 587-92.
10. Y. Fukuda and M. Kumon: in *Thermal Spraying: Current Status and Future Trends,* A. Ohmori, ed., High Temperature Society of Japan, 1995, pp. 107-11.
11. G.Y. Lai: *Thin Solid Films,* 1978, vol. 53, pp. 343-51.
12. J. He, M. Ice, and E.J. Lavernia: *Nanostr. Mater.,* 1998, vol. 10, pp. 1271–83.
13. X.D. Liu, M. Nagumo, and M. Umemoto: *Mater. Trans., JIM,* 1997, vol. 38, pp. 1033-39.
14. C. Suryanarayana, D. Mukhopadhyay, S.N. Patankar, and F.H. Froes: *J. Mater. Res.,* 1992, vol. 7, pp. 2114-17.
15. D.A. Konstantinidis and E.C. Aifantis: *Nanostr. Mater.,* 1998, vol. 10, pp. 1111-18.
16. Z.N. Farhat, Y. Ding, D.O. Northwood, and A.T. Alpas: *Mater. Sci. Eng.,* 1996, A206, pp. 302-13.
17. G.Y. Lai: *Thin Solid Films,* 1979, 64, pp. 271–80.
18. G.Bank, T. Schmit, P. Ettmayer, and B. Lux: in *Binary Alloy Phase Diagrams,* 2nd ed., T.B. Massalski, ed., ASM International, Materials Park, OH, 1990, pp. 1304-05.
19. *Lange's Handbook of Chemistry,* 13th ed., J.A. Dean, ed., McGraw-Hill Book Company, New York, NY, 1985, pp. 9-19.